Journal of Power Sources 434 (2019) 226735

Contents lists available at ScienceDirect

Journal of Power Sources

journal homepage: www.elsevier.com/locate/jpowsour

Lifetime assessment of solid-state hybrid supercapacitors based on cotton fabric electrodes

A.J. Paleo [a,*], P. Staiti [b], A.M. Rocha [a], G. Squadrito [b], F. Lufrano [b,**]

[a] 2C2T – Centro de Ciência e Tecnologia Têxtil, Universidade do Minho, Campus de Azurém, 4800-058, Guimarães, Portugal
[b] CNR-ITAE, Istituto di Tecnologie Avanzate per l'Energia "Nicola Giordano", 98126, S. Lucia, Messina, Italy

HIGHLIGHTS

- Hybrid cotton fabric electrodes with MnO_2 and AC by easy processes were developed.
- A new assessing method for long-term durability under harsh conditions is analysed.
- The use of Aquivion as solid-state electrolyte in SCs is introduced for first time.
- The hybrid solid-state supercapacitors worked with success in a high voltage range.
- The supercapacitors showed low self-discharge rates and good specific capacitances.

ARTICLE INFO

Keywords:
Carbon nanofiber
Manganese oxide
Solid-state electrolyte
Hybrid supercapacitor

ABSTRACT

Electrodes based on activated carbon and manganese oxide coated on a cotton woven fabric were developed and investigated. The electrodes were then assembled with two polymer electrolyte membranes, Nafion®115 and Aquivion®E87-05S, and two different supercapacitors were produced with specific capacitances and energy densities of 130 and 132 F g^{-1}, and 11.5 and 11.7 Wh kg^{-1}, respectively. Furthermore, a new durability methodology, which combines galvanostatic charge/discharge cycles together with potentiostatic floating conditions, was used to get insight into their electrochemical performance under stringent conditions. The supercapacitor assembled with Nafion®115 electrolyte worked successfully for 10 k cycles and 140 h under a constant voltage of 1.6 V (floating condition), whereas the supercapacitor assembled with Aquivion®E87-05S electrolyte worked successfully for more than 15 k cycles and 210 h, without any appreciable degradation of their electrochemical properties. In summary, hybrid solid-state supercapacitors based on electrodes produced by simple methodologies and low-cost materials, and with long durability performance under very harsh conditions were developed and analysed for their potential utilization as flexible energy storage devices.

1. Introduction

At present, batteries and electrochemical capacitors are becoming of primary importance as power supplies of portable electronic systems. However, these devices are rigid and have limited usability in terms of mechanical stability upon bending or stretching for wearable electronics. In this respect, textile fabrics, which are thin flexible sheets of interlaced yarns produced by different technologies such as weaving, knitting, and braiding have additional advantages over other materials owing to their mechanical strength, flexibility properties and absorption and desorption ability (for absorbing and releasing of ions in the solvent) [1], and therefore, flexible energy storage devices based on textile fabrics, particularly oriented towards the production of supercapacitors (SCs), are a viable alternative to overcome those limitations because of their quick charge-discharge capability, long life and safety. It is generally accepted that energy in SCs is electrostatically stored by accumulated charges on the electrode surface, and electrolyte ions with counterbalancing charge on the electrolyte side, which is denominated as electric double layer capacitance (EDLC) [2]. However, the fabrication of scalable, lightweight and durable textile-based SCs possessing a combination of high capacitance with high power and energy density is still a significant challenge [3], and fabric-based electrodes with high

* Corresponding author.
** Corresponding author.
E-mail addresses: ajpaleovieito@2c2t.uminho.pt (A.J. Paleo), lufrano@itae.cnr.it (F. Lufrano).

https://doi.org/10.1016/j.jpowsour.2019.226735
Received 18 March 2019; Received in revised form 14 May 2019; Accepted 5 June 2019

electronic conductivity thanks to the incorporation of carbon nanostructures such as carbon nanotubes (CNT) [4], graphene [5,6], and/or a combination of them [7] by different methodologies [8], have been recently proposed for the design of SCs. Nevertheless, the electrochemical properties of the above mentioned carbon nanostructures are still limited. In this regard, it is well known that charge storage can be increased in supercapacitors with pseudocapacitance, i. e. fast surface redox reactions, which occur at or near the surface of carbon materials, conducting polymers [9] and transition metal oxides [10]. Consequently, activated carbon (AC) with mesoporous structures [11] together with pseudocapacitive metal oxides such as manganese oxides (MnO_x) [12], are frequently added to the fabric-based electrodes to enhance their electrochemical properties. On the other hand, cotton-based textiles are drawing strong attention among natural fiber textile fabrics to act as wearable platform for textile supercapacitors [13,14]. The current research in the development of textile supercapacitors can be separated into two main lines of investigation, bottom-up and top-down. In the bottom-up approach, natural or synthetic fibers are transformed into electrode fibers by different methodologies, and so they can be interlaced in a subsequent step to produce energy storage devices [15,16]. On the contrary, in the top-down approach already final product textile fabrics are transformed into energy storage devices. The first work reporting this type of top-down approach with cotton fabric has been conducted by Yi Cui research group in 2010 [17]. In that work, dip-coated CNT cotton fabric electrodes electrodeposited with MnO_2 were studied for producing hybrid SCs with excellent cycling stability and specific capacitances of around 125 F g^{-1} in the working voltage range of 0.8 V. The use of cotton fabric as the starting material of the electrodes for SCs have been also investigated in some other relevant works. For instance, polypyrrole (PPy) nanorods were deposited on cotton fabrics, and the obtained fabrics could be directly used as supercapacitor electrodes, with a maximum specific capacitance of 325 F g^{-1} in the working voltage range of 0.8 V, and an energy density of 24.7 Wh kg^{-1} [18]. In another recent work, electrodes were produced with multiwall carbon nanotubes (MWCNT) and reduced graphene oxide (rGO) deposited by vacuum filtration on nickel coated cotton fabric. The electrodes were then assembled with a cotton fabric separator in 5 M LiCl aqueous electrolyte solution. The final SCs achieved a specific capacitance of 262 F g^{-1} at 0.84 A g^{-1} in the working voltage range of 0.8 V, and an unexpected increment of 18% in their specific capacitance after 10 K cycles [19]. On the other hand, the good performance of SCs depends also of the type and conductivity of the electrolyte used, which has the double function of working as separator between the electrodes and transport of electrolyte ions when it has the form of gel or polymer [20,21]. Since aqueous electrolytes show practical disadvantages in wearable SC devices due to liquid leakage, there is an increasing interest in replacing them with polymer/gel electrolytes [22]. For instance, a solid-state flexible and asymmetric supercapacitor with PVA/LiCl gel, MnO_2 nanowires and Fe_2O_3 nanotubes grown on carbon fabric electrodes, with 91.3 F g^{-1} (2 mA cm^{-2}) in the working voltage window of 1.6 V, a capacitance retention of 95.2% after 3K cycles, and values of resistances between 3.9 and 7.6 Ω cm^2 during cycling stability test, was already reported [23]. In another work, SCs assembled with electrodes of $NiCo_2O_4$@$NiCo_2O_4$ core/shell nanostructures grown on cotton activated carbon textiles and PVA/KOH, achieved a specific capacitance of 60 F g^{-1} (100 mA cm^{-2}) in the working voltage of 1.6 V, a resistance of around 1.5 Ω cm^2, and capacitance retention of 100% after 1 k cycles [14]. It was also recently reported the use of large-area flexible electrodes based on a polyester textile, rGO and PANI, and PVA/H_3PO_4 as gel electrolyte, to assemble a SC with 152 F g^{-1} (0.5 mA cm^{-2}) in the voltage window of 0.8 V, and retention of 85.9 % after 1 k cycles [24]. However, the PVA based solid electrolytes used in the above referenced works present also some relevant unresolved issues such as their high resistivity, the difficulty of controlling with precision their thickness during the fabrication of the SC, which can worsen the adhesion between electrode and electrolyte, and the selection of appropriate current collectors to avoid corrosion when using alkali or acid electrolytes. Furthermore, PVA based gel electrolytes in acidic and alkaline environments cannot be used with MnO_2 based electrodes because of the poor chemical stability of MnO_2, and they cannot achieve voltage windows above 1.23 V (vs NHE) because of the water decomposition, which causes very high self-discharge rate. It is in this context that we have selected the perfluorosulfonate (PFSA) Nafion®115 and Aquivion®E87-05S membranes as solid polymer electrolytes for the design and fabrication of our SCs because of their high ionic conductivities, even as cation exchange membranes in sodium form (i.e. Na^+) at pH ≈ 7, wide voltage window stability (i.e. 1.6 V), controlled thickness, outstanding mechanical strength, and low self-discharge rate [25]. These polymer electrolytes are currently employed in polymer electrolyte membranes (PEMFCs) and direct alcohol (DAFCs) fuel cells because of the outstanding properties above numbered [26]. Some initial interesting characteristics of Nafion®115 electrolyte were already discussed in our previous work, where asymmetric SCs based on AC/MnO_2 deposited onto dip-coated carbon nanofiber cotton fabric electrodes were designed, fabricated and analyzed [27]. In the present work, we extend the application of PFSA polymer electrolytes and optimize the preparation in a single-step of MnO_2 and AC cotton fabric electrodes for the fabrication of two asymmetric solid-state SCs with Nafion®115 and Aquivion®E87-05S electrolyte membranes (Table 1). Furthermore, a new practical test procedure for the long-term durability assessment of asymmetric and hybrid SCs under stringent conditions, which include cycles with the combination of galvanostatic charge/discharge (G-CD) and potentiostatic floating conditions, is analysed and discussed. As far as the authors are aware, this is the first work that reports the study of a SC with the Aquivion E87-05S solid polymer electrolyte, and the lifetime assessment of solid-state SCs by using this new type of accelerated stress test method.

2. Experimental section

2.1. Materials

100% cotton woven fabric with 14.9 × 20.2 warp x weft yarn linear density (tex) and 0.26 mm thickness at 18 Pa provided by a local company, was used without any type of pre-treatment as base-substrate of the electrodes. A combination of activated carbon (AC) *Norit A Supra Eur* with a specific surface area of 1500 m^2 g^{-1}, vapour grown carbon nanofibers (CNF) *Pyrograf III PR 24 LHT XT* with diameters of around 100 nm and lengths ranging from 50 to 100 μm, carbon black (CB) *Shawinigan acetylene black,* and dry powder manganese oxide (MnO_2) prepared by a simple co-precipitation method based on chemical reaction in aqueous solution [28], were used for producing the corresponding active layers with conducting and electrochemical properties. *Nafion® 115 DuPont* and *Aquivion® E87-05S* with a thickness of 125 and 50 μm, and equivalent weight (EW) of 1100 and 865 g mol^{-1}, respectively, were employed as polymer electrolyte membranes. All the other materials used in this work were purchased from Sigma-Aldrich and used without further purification.

2.2. Preparation of electrodes and supercapacitors

Two different types of electrically conducting and hybrid composite electrodes based on MnO_2 (positive electrode) and AC (negative electrode) were produced. The MnO_2 based electrodes were prepared by spreading onto the cotton fabric samples a slurry composed of: 70 wt% of MnO_2, 10 wt% of CB, 10 wt% of CNF, 10 wt% of poly(vinylidene fluoride) (PVDF) binder and N,N dimethylacetamide (DMAc) solvent, whereas the composition for the AC based electrodes was: 80 wt% of AC, 10 wt% of CNF, 10 wt% of PVDF and DMAc. All the electrodes were dried first at 70 °C for 24 h, and then a further heat treatment, which involved 1 h at 120 °C and 20 min at 160 °C, was carried out to improve their mechanical strength. At the end, all the electrodes were hot-

Table 1
Description of electrodes and final solid-state supercapacitor compositions.

Supercapacitor name	Positive electrode		Negative electrode		Electrolyte
	Composition (wt%)	Thickness/Active Mass	Composition (wt%)	Thickness/Active Mass	
Cotton@Nafion Cotton@Aquivion	MnO_2 (70%), CB (10%), CNF (10%), PVDF (10%)	150 μm/2.15 mg cm^{-2}	AC (80%), CNF (10%), PVDF (10%)	175 μm/2.56 mg cm^{-2}	Nafion®115 Aquivion®E87-05S

pressed at 160 °C and 40 bar during 10 min with the aim of increasing their electrical conductivity, and a positive to negative electrode mass ratio of 0.84 was achieved. The electrodes were then cut in circular shapes of 2 cm^2, whereas the Nafion®115 and Aquivion®E87-05S membranes were cut slightly larger than 2 cm^2 (around 2.5 cm^2) to prevent lateral electrical short circuits. The SCs were assembled with the Nafion®115 and Aquivion®E87-05S membranes and two different types of SCs, named as *Cotton@Nafion* and *Cotton@Aquivion*, were produced. The electrodes were impregnated with 1 M Na_2SO_4 solution, whereas the Nafion®115 and Aquivion®E87-05S membranes were exchanged in Na^+ form by immersion for 18 h in 1 M Na_2SO_4 solution under slow stirring, before assembling. Further specific details of the electrodes are shown in Table 1.

2.3. Materials characterization

Morphological analysis of the as-prepared electrodes (fresh electrodes) and the aged electrodes was performed in an Ultra-high resolution Field Emission Gun Scanning Electron Microscopy (FEG-SEM), FEI Company. The aged electrodes were dried at room temperature for some days, and then cut in small samples of about 0.5 cm^2, which were fixed to the SEM sample holder by a conductive tape. The samples were gold coated with a thin film (about 20 nm) in a cold sputter coater. The SEM analyses were carried out at 5 kV and 20 kV of accelerating voltage and at different magnifications by scanning the whole area of each sample. Energy dispersion of emitted x-ray (at 20 kV) was used to verify the uniformity in the composition of the different samples.

X-ray photoelectron spectroscopy (XPS) of cotton based fresh and aged electrodes was recorded by a Physical Electronics (PHI) 5800-01 spectrometer. Each spectrum was obtained by using pass energies of 58.7 eV, for the elemental analysis, and 11.75 eV for the determination of the oxidation states and chemical compositions. A scan analysis was carried out for producing a survey spectrum ranging from 0 eV to 1200 eV, which was used to determine the elemental surface composition. High-resolution scans were also carried out for Mn 2p, Mn 2s, C 1s and O 1s to complete the surface analysis of electrodes. Different samples based on AC (negative electrodes) and MnO_2 (positive electrodes) were calibrated with C1s (284.6 eV) peak. The areas of peaks were estimated by calculating the integral of each peak after subtracting the background noise and fitting the experimental peaks by the Gaussian function.

2.4. Electrochemical characterization

The supercapacitors with 2 cm^2 circular-shape two-electrodes were investigated in a titanium cell connected to Autolab/Metrohm PGSTAT 302/FRA2 (Eco Chemie, Netherlands) potentiostat-galvanostat electrochemical workstation. The cyclic voltammetry (CV) tests were carried out in potentiodynamic mode at different voltage sweep rates (5, 10, 50 and 100 mV s^{-1}) and voltage ranges from 0 to +1.6 V and vice versa. The galvanostatic charge/discharge tests (G-CD) were carried out in the same voltage range (0 to +1.6 V) and at constant currents of ±0.2, ±0.5, ±1 and ±2 A g^{-1}. The electrochemical impedance spectroscopy tests (EIS) were performed at open circuit voltage (OCV), with voltage sine wave amplitude of 10 mV, and frequencies from 1 mHz to 500 kHz by using the PGSTAT 302 potentiostat equipped with the FRA2 module.

3. Results and discussion

3.1. Morphology and structure of fresh electrodes

The scanning electron microscopy images of composite electrode samples before electrochemical tests (fresh electrodes) are shown in Fig. 1. The positive electrode (Fig. 1a) is composed of spherical MnO_2 nanoparticles, carbon black particles with irregular shapes and large sizes, and carbon nanofibers. All these particles and nanofibers were coated successfully on the woven cotton fabric. The MnO_2 nanoparticles appear uniformly distributed, while CB particles showed larger agglomerates with micrometric sizes. CNF have the main function of connecting the MnO_2 and CB particles, thus creating the necessary conductive paths for electronic transport. The negative electrode (Fig. 1b) showed a non-uniform distribution of AC particles in the micrometric scale range with some entangled CNF. The electronic conduction paths are also ensured by the contacts between AC particles and CNF. Overall, these fresh electrodes coupled with the sodium exchanged PFSA membranes allowed the production of solid-state SCs with excellent electrochemical characteristics.

X-ray photoelectron spectroscopy was also performed to evaluate the surface chemical composition of the fresh electrodes, and the results are shown in Fig. 1c. The full survey-scan spectrum of the positive electrode (Fig. 1c red line) shows that it is composed of four main elements: Mn, O, C and F. The fluorine comes from the PVDF inert binder and hence it is not further considered. The two peaks at 642 eV (Mn $2p_{3/2}$) and 653.8 eV (Mn $2p_{1/2}$), with an energy separation of 11.8 eV, showed that Mn^{4+} is the prevailing species on the surface [29,30]. The C 1s peak at 284.6 eV is due to the CB particles and the CNF, while the O 1s peak at 631.5 eV has its origin in the oxygen provided by the Mn oxides and surface oxygenated groups of the carbon materials. The whole survey spectrum of the negative fresh electrode (Fig. 1c blue line) shows only the presence of C, O and F elements. Further XPS examination comparing the fresh and the aged electrodes will be discussed in the later sections.

3.2. Electrochemical analysis at initial conditions

The electrochemical analyses of both SCs at initial conditions obtained by CV at different voltage sweep rates from 5 to 100 mV s^{-1} are plotted in Fig. 2a and c. The current density and specific capacitance were calculated from the sum of active masses from both electrodes, (4.30 mg from MnO_2 and 5.12 mg from AC). The original values of the current (I) in the voltammograms were converted in specific capacitance (Cs) per one electrode mass by using the equation C (F g^{-1}) = 4 x [I (A)/dV/dt (V s^{-1})]/[mass active materials of capacitor (g)]; where dV/dt is the scan rate. The Cotton@Nafion SC shows slightly higher capacitance than the Cotton@Aquivion SC. In particular, the Cotton@Nafion SC showed specific capacitances close to 100 F g^{-1} and nearly rectangular shapes in the whole range of voltage scan rates. The quasi-rectangular shapes observed in Fig. 2a–c show a high stability at operating voltage of 1.6 V, which is an important finding because it demonstrates the absence of evident oxygen (OER) and hydrogen (HER) evolution reactions in the electrodes [31,32]. In fact, the operation voltage of 1.6 V in both SCs exceeds the thermodynamic potential window of water decomposition (e.g. 1.23 V, vs NHE) at room temperature. The

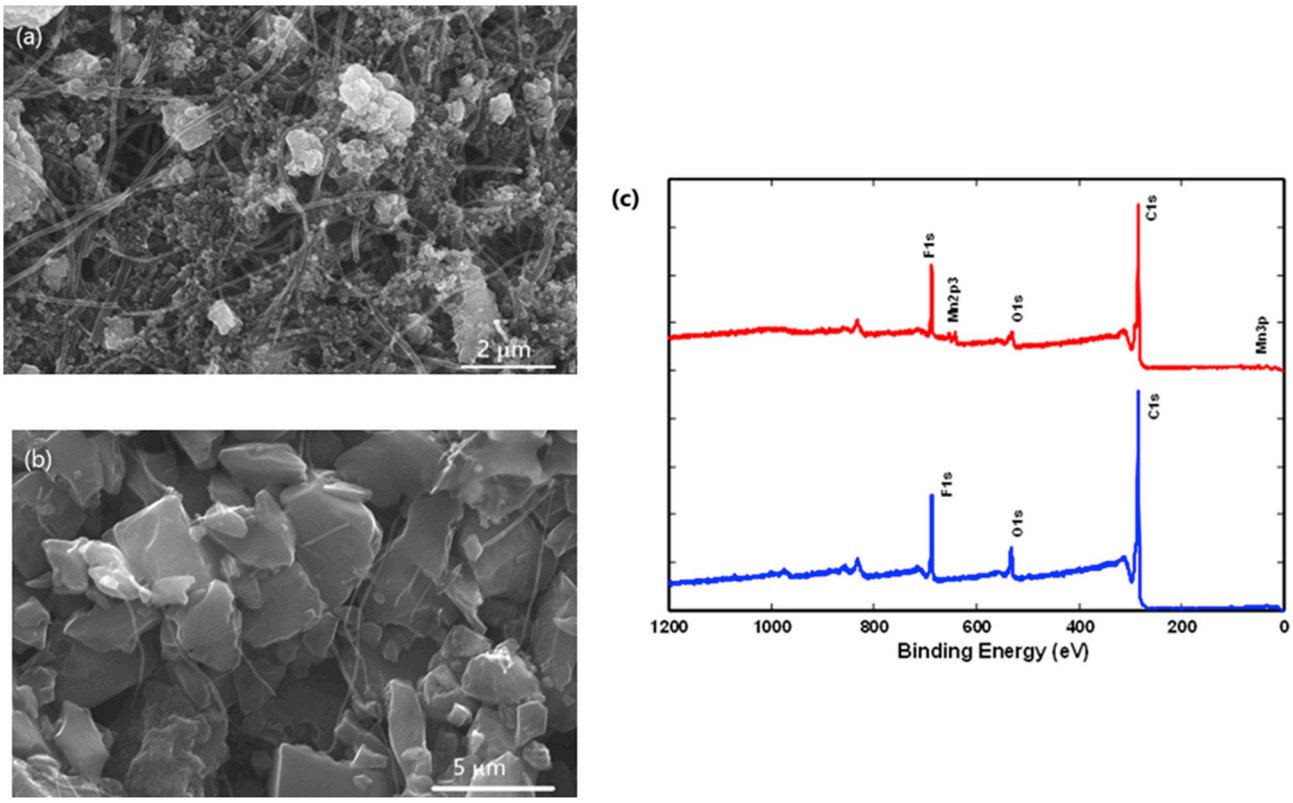

Fig. 1. SEM images of the upper surface. MnO_2 based electrode (a), AC based electrode (b). XPS survey spectra (c): MnO_2 based electrode in red line, and AC based electrode in blue line. (For interpretation of the references to colour in this figure legend, the reader is referred to the Web version of this article.)

voltammograms of the Cotton@Aquivion SC showed less perfect rectangular shapes in the same voltage range, probably due to its higher distributed ionic resistances, as it is confirmed by the EIS analysis (Fig. 2e). Despite the presence of MnO_2 in their positive electrodes, there is no any evidence of Faradaic processes in both SCs at the initial conditions, which can be explained because of those processes happen very fast in the whole cell [33,34]. In general, both SCs show in their voltammograms the quasi-rectangular shapes typically observed in electrodes with the electrical double layer capacitance (EDLC) behaviour [27,35], even at the highest scan rates of 100 mV s^{-1}. Fig. 2b and d show the G-CD curves of Cotton@Nafion and Cotton@Aquivion SCs in the voltage range from 0 to +1.6 V. We observed a retention in capacitive performances of around 75% and 70% in supercapacitors with Nafion and Aquivion, respectively, when current increased from 0.2 to 2 A g^{-1} in G-CD tests. This is an expected result if we consider that pseudocapacitive processes, which involve a fast transfer of electrons on the surface of MnO_2, are occurring [36]. Both SCs show high columbic efficiency and triangular shapes with low voltage drops (iR drop) occurring during the current inversion, associated with the over potential caused by the charge redistribution through the electrodes [37]. In summary, a similar to EDLC behaviour with low electrical resistivity and excellent capacitance is confirmed in both SCs from the analyses of their voltammograms and G-CD curves at initial conditions, which practically emulate the behaviour of electrostatic capacitors but with much higher capacitances (e. g. >100 F g^{-1}).

The Nyquist plots of both SCs at initial conditions are reported in Fig. 2e. The inset shows the high frequency region. The plots are very similar at high and very low frequency, while they show differences at intermediate frequencies where the more resistive character of Aquivion is evident. The high frequency semicircles observed in both supercapacitors were fitted by R_S ($R_{CT}C_{PE}$) equivalent circuit, in which R_S is the electrolyte resistance, R_{CT} is the charge transfer resistance and C_{PE} or Q is the constant phase element, defined as the circuit element to be used in EIS analysis when the electrodes have some roughness and high porosity [38], and a non-ideal behavior of the electric double layer have to be considered. Values of R_S equal to 0.82 and 0.78 Ω cm^2 have been calculated for Cotton@Nafion and Cotton@Aquivion SC, respectively, which evidence very low resistivities of both Nafion®115 and Aquivion®E87-05S membranes and fast charge propagation through electrodes (see inset of Fig. 2e). Furthermore, the Cotton@Nafion SC (R_{CT} = 2.6 Ω cm^2) exhibits interfacial resistances with lower radius than the Cotton@Aquivion SC (R_{CT} = 3.9 Ω cm^2). This latter supercapacitor also shows higher distributed resistances in the middle frequency range (Hz), while the differences between the impedances of both SCs are less pronounced at low frequencies (mHz), and finally the results overlap near to 1 mHz.

3.3. Lifetime analysis under accelerated stress test

The electrochemical characterizations of both hybrid solid-state SCs in a neutral aqueous system at initial conditions have shown high specific capacitances and low resistivities in a wide voltage window of 1.6 V, as it was discussed in the previous section. On the other hand, we propose a different methodology for the long-term durability assessment of our supercapacitors. This test-method allows monitoring the ageing behaviour of SCs through a combined procedure of cycling and floating method, which can simulate better their lifetime and state-of-health (SoH) under stringent environments. Specifically, the SCs are subjected to G-CD sequences consisting of an initial galvanostatic charge phase at 2 A g^{-1}, a potentiostatic phase for 50 s at constant voltage of 1.6 V (floating condition), and a final galvanostatic discharge phase at −2 A g^{-1}, as it is shown in Fig. 3. Though, the floating methodology was already proposed for testing the stability of non-aqueous [39,40] and aqueous [41] based supercapacitors, this combination of cycling and floating is presented for the first time with this study. This methodology is repeated up to 15 k cycles during which the ageing behaviour was

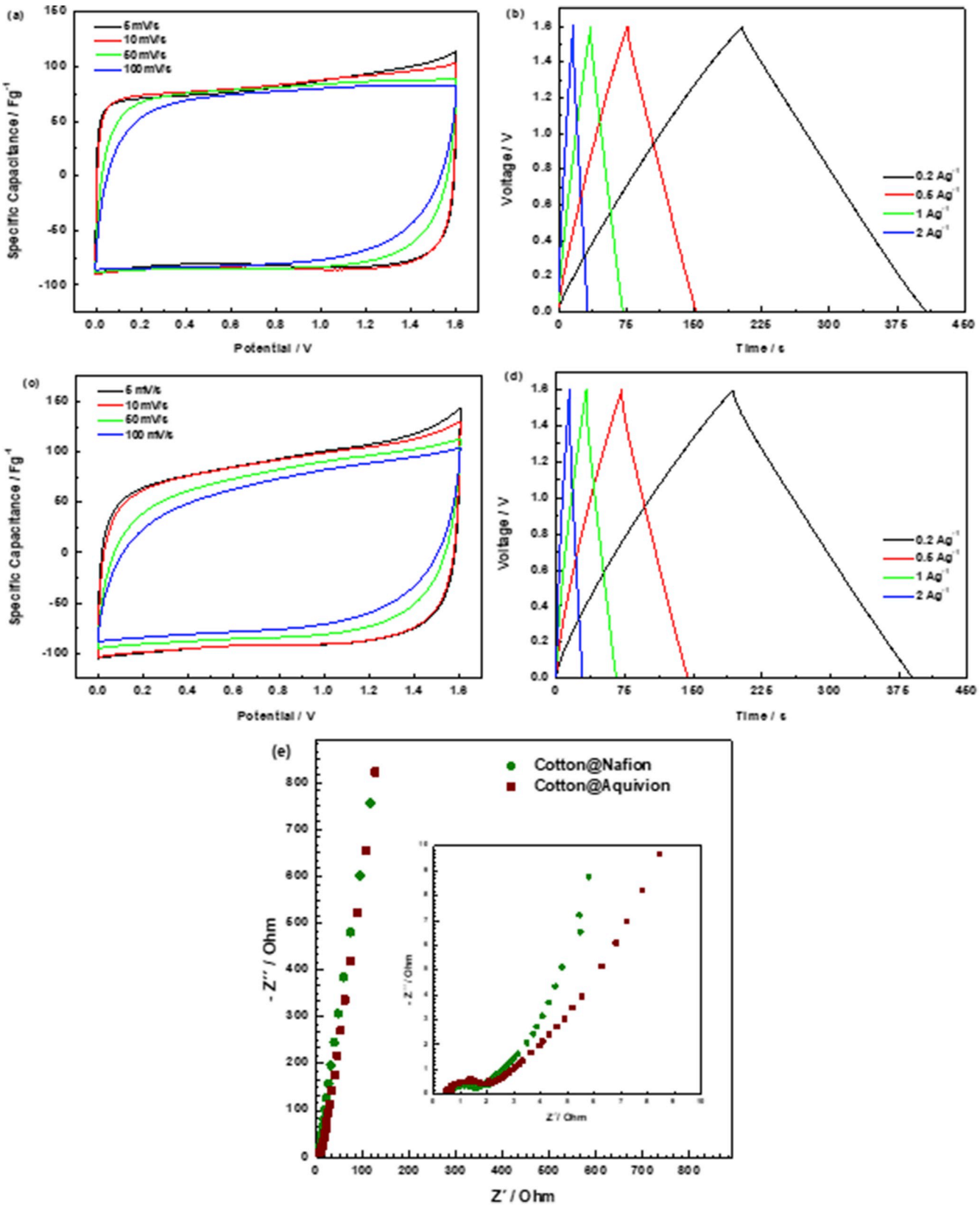

Fig. 2. Specific capacitance versus cell voltage at scan rates from 5 mV s^{-1} to 100 mV s^{-1}, and G-CD at current densities from 0.2 A g^{-1} to 2 A g^{-1}. Voltammograms (a) and G-CD (b) of Cotton@Nafion SC. Voltammograms (c) and G-CD (d) of Cotton@Aquivion SC. Nyquist plots of the two hybrid SCs at initial conditions (e).

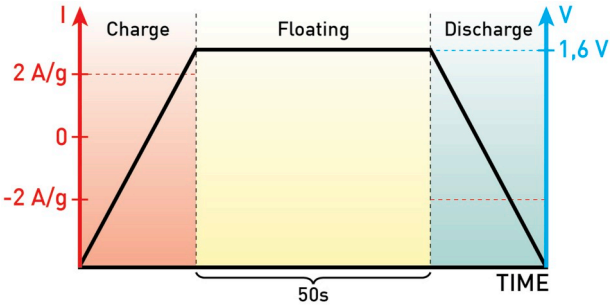

Fig. 3. Typical cycle of stability that includes combined G-CD at ± 2 A g^{-1} with potentiostatic floating at 1.6 V during 50 s.

monitored by different control tests (CV at 5 mV s^{-1}, G-CD at 0.2 A g^{-1} and EIS) carried out at intermediate number of cycles (e.g. 0, 2 k, 5 k, etc.) as provided in Figs. 4 and 5.

The initial voltammograms exhibit rectangular shapes especially in Cotton@Nafion SC, while the Cotton@Aquivion SC shows higher resistive effects, and as far as the number of cycles are progressing (Fig. 4a and c) deviations from these initial behaviours are observed. For instance, a broad hump above 5 k cycles during charge and discharge voltammetries is clearly manifested for Cotton@Nafion SC. On the contrary, the voltammograms of Cotton@Aquivion SC proceed more regularly and flat humps can be observed only after 10 k cycles. Furthermore, it is possible to observe how the inversion of the sign of the current at 1.6 V and 0 V is practically instantaneous during all voltammetries (Fig. 4a and c). This means that both SCs still show low resistance, while at the same time their capacitances increase as the number of cycles move forward, as it is observed from the negative/positive areas, which are higher than the areas of the starting cycles. In conclusion, there is not any deterioration detected from CV at high number of cycles, and the discharge time after 10 and 15 k cycles for both SCs are also higher than initial (G-CD Fig. 4b and d). These trends and results were not expected because our supercapacitors include the MnO_2 as the pseudocapacitive material in positive electrodes, and during the tests, the electrodes and electrolytes were subjected to severe conditions. We have reported similar achievements in a previous work [27], though in that work the cycles were performed with a lower stringent methodology, and consequently the results showed here on the long-term durability of this type of SCs provide a new scientific finding.

The progression of the durability tests and the state-of-health of both SCs were also monitored by in-situ EIS and their representative Nyquist and Bode plots are shown in Fig. 5. The Nyquist plots of both SCs at high frequencies (kHz range), described in the insets of Fig. 5a and c, demonstrate a small increase in their whole resistance, which includes the electrolyte, the electrode/collectors and the electrolyte/electrodes resistances, with the progression of the cycles. In addition to the mentioned resistances, the charge transfer resistance, R_{CT}, due to the diffusion of the charges (i. e. ions and electrons) through the electrodes has also to be included in that whole resistance increase. The absence of low frequency semicircles (mHz range) indicates that accentuated redox processes were not detected in both SCs even over a long time-scale of

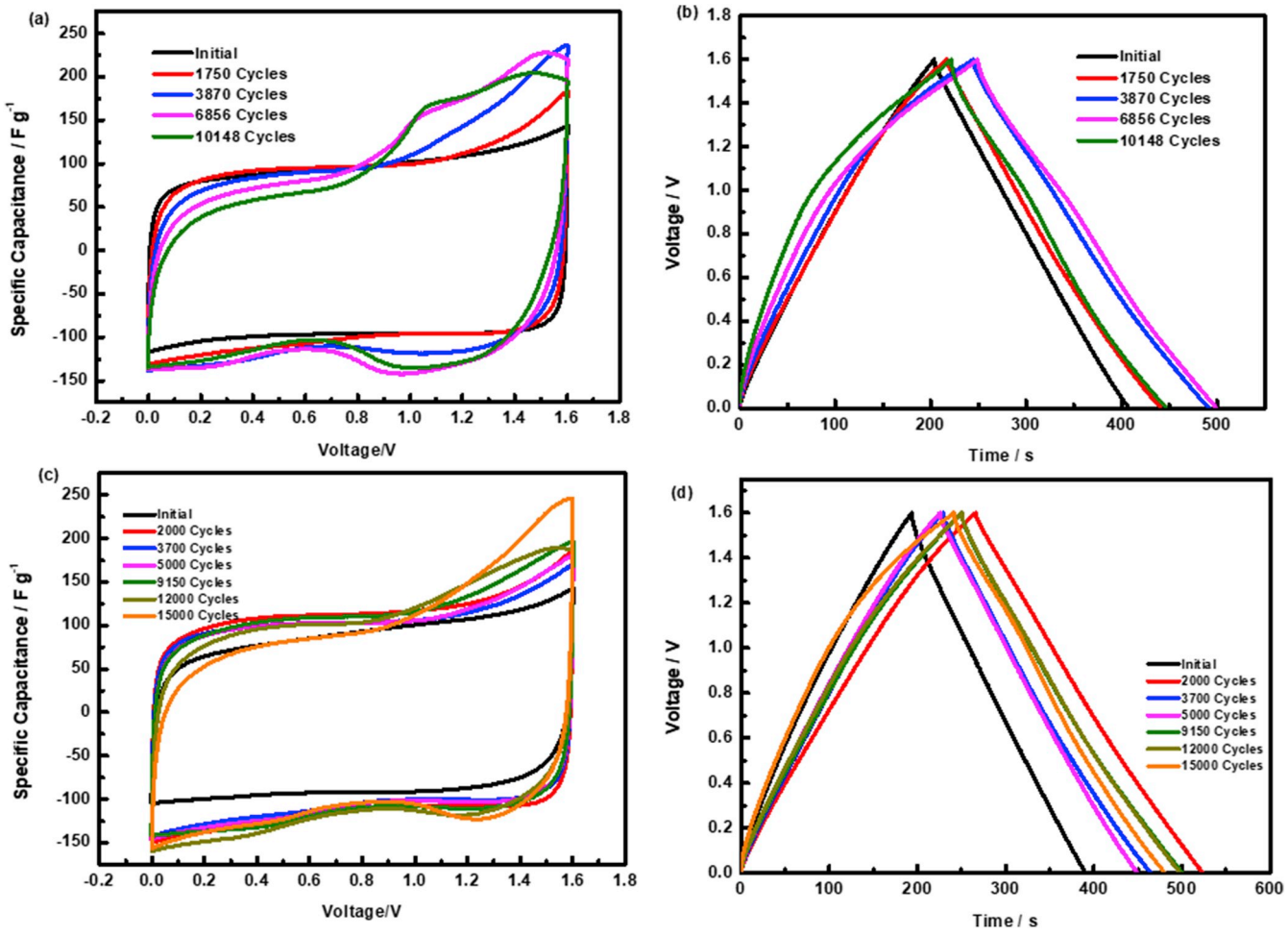

Fig. 4. Specific capacitance versus cell voltage at 5 mV s^{-1} and G-CD at 0.2 A g^{-1} of long-term durability tests. Voltammograms (a) and G-CD (b) of Cotton@Nafion SC. Voltammograms (c) and G-CD (d) of Cotton@Aquivion SC.

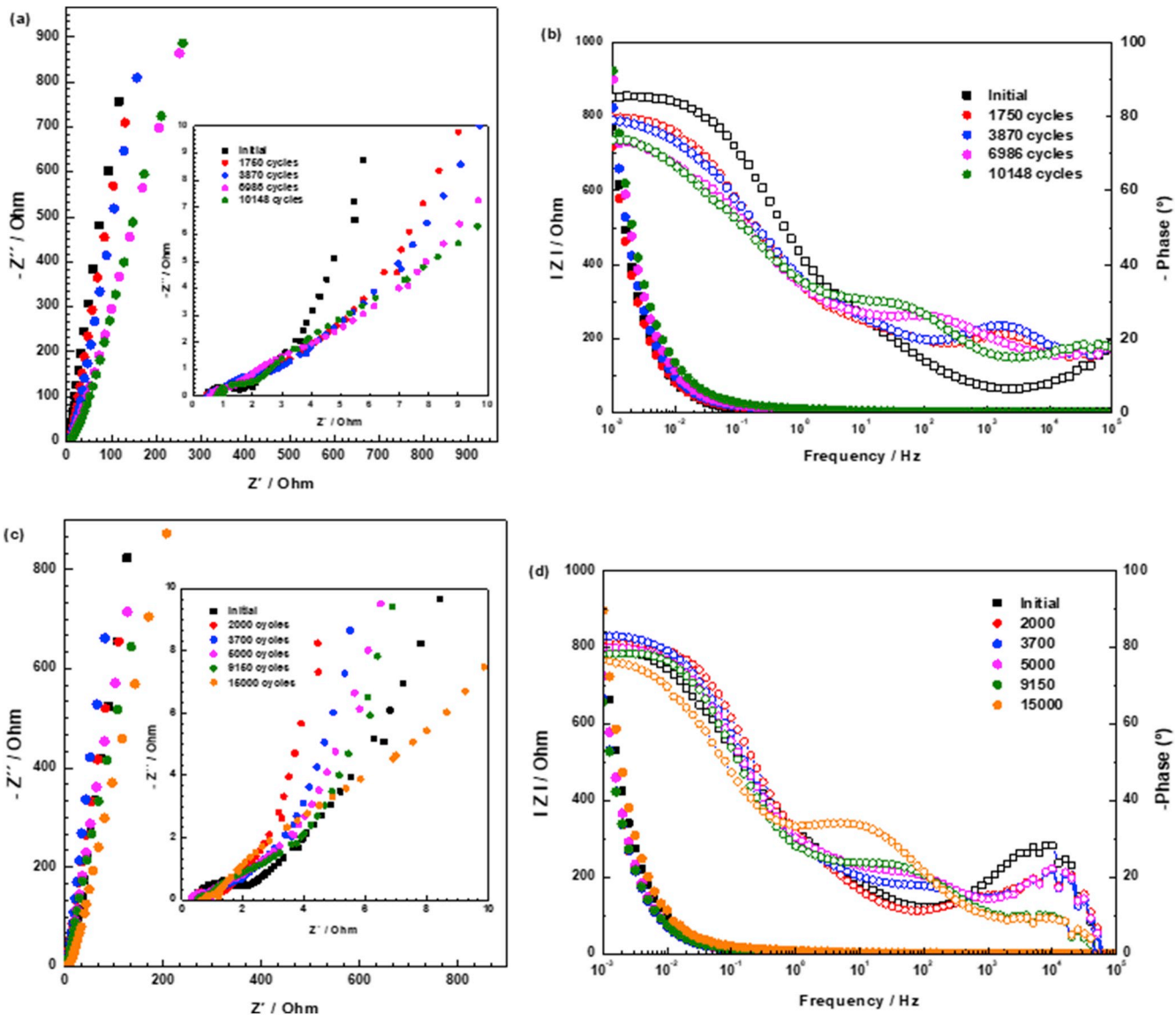

Fig. 5. Long-term durability EIS of Cotton@Nafion (top) and Cotton@Aquivion SC (bottom). Nyquist plots (the inset shows the high-frequency region) (a) and (c); Bode plots (absolute impedance is the solid symbol and the phase angle is the open symbol) (b) and (d).

measurement (1 mHz is equivalent to 1000 s). Furthermore, the data points almost vertically situated on the left part of Nyquist plots (Fig. 5a and c) show that both cells behave as quasi-ideal capacitors with a slight frequency dependence caused by the increase of R_{CT} during the progression of cycles. The Bode plots of SC at the initial condition (Fig. 5b and d) show that both cells resemble quasi-ideal capacitors with phase-shift angles very close to −90° (i. e. ideal EDLC behaviour) and then, as the number of cycles is increasing, the phase-shift angles decrease up to about −75° with a behaviour closer to a pseudocapacitor [42]. It must be reminded that a phase-angle of −80° was proposed as an indicator to distinguish a capacitor from a non-capacitor like behaviour [42,43], though this statement has not gained a general consensus. Taking that indicator into consideration, our study shows a change from an ideal EDLC to pseudocapacitor (Fig. 5b and d) as the number of cycles runs forward. Furthermore, a broadening of the phase peaks from higher to lower frequencies, particularly in the Cotton@Aquivion SC, is observed with the increase of number of cycles. These modifications may be associated with the appearance of some slower redox process in MnO_2 based electrodes, which have also been detected in the voltammograms of both SCs (Fig. 4a and c). In summary, both SCs showed good capacitive behaviour and high electrochemical performance despite the cells were subjected to very stressful ageing conditions. For instance, the Cotton@Nafion SC was subjected to 10 k G-CD cycles, which includes a potentiostatic floating phase of approximately 140 h at 1.6 V. These are exceptional results if we consider that low-cost materials such as AC, MnO_2 and electrical insulating cotton woven fabric were utilized in the production of the electrodes.

The morphology of aged electrodes was analyzed by SEM to further investigate the effects of accelerated ageing tests and it is shown in Fig. 6. The electrodes were just dried, without any type of washing, in order to avoid any undesired alteration of the samples before the SEM analysis. Fig. 6a and c show evident white large particles of deposited Na_2SO_4 salt electrolyte and they do not show clearly any particle growth corresponding to MnO_2. The Fig. 6a shows also some effect of fusing or coarsening among MnO_2 particles corresponding to the positive electrodes of Cotton@Nafion SC, though they remained in the nanometric range. A flattening effect caused by the pression of the electrodes against the membranes in the cell, that slightly alters their morphology, can be clearly observed in the disassembled aged positive electrodes, when compared with the fresh ones (Fig. 1a). Apart from that, the SEM images of the fresh and the aged positive and negative electrodes of both SC do not show any significant change in their morphological appearance.

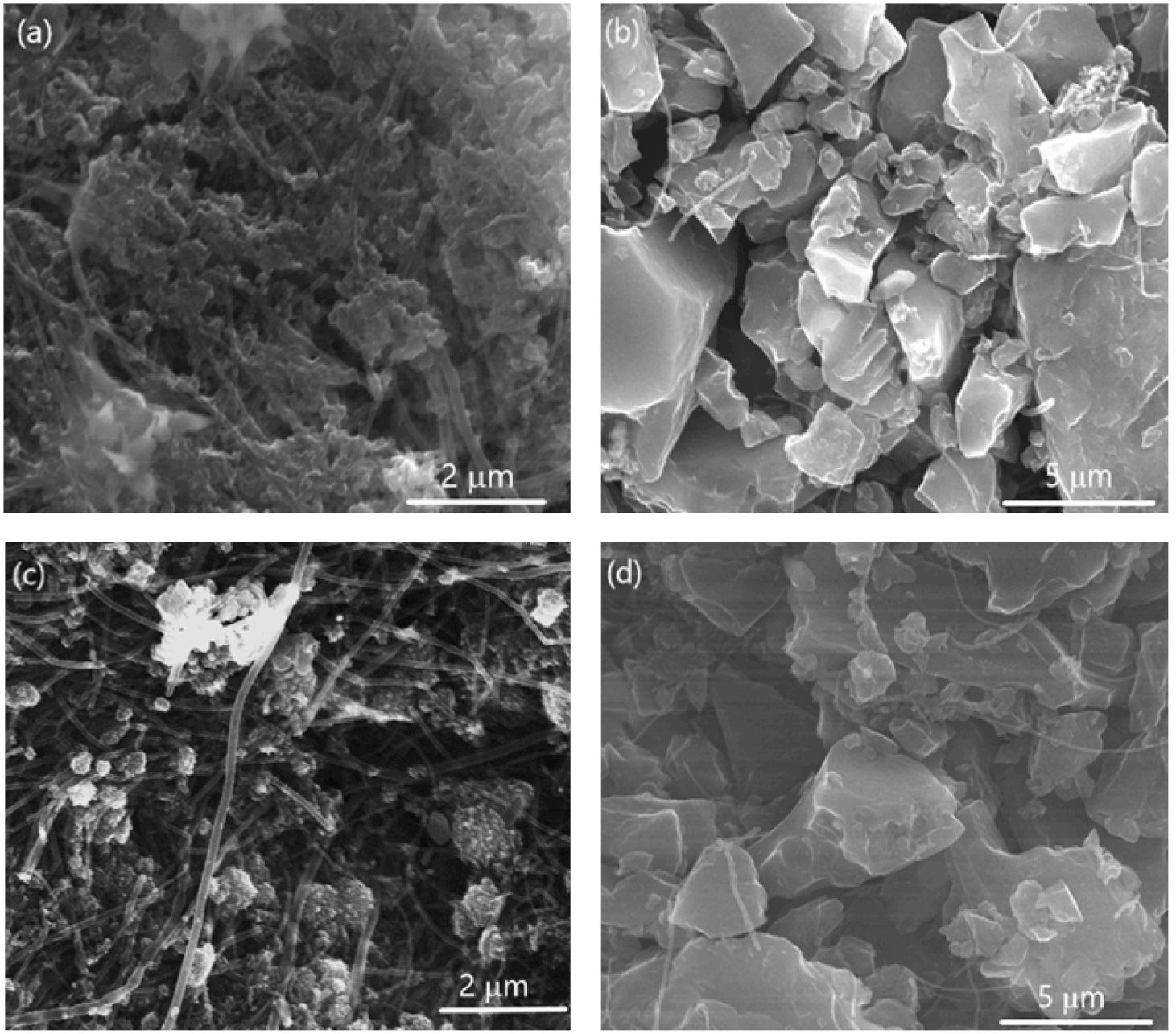

Fig. 6. SEM images of electrodes after accelerated ageing tests. Positive electrodes used with Nafion®115 (a) and Aquivion®E87-05S (c). Negative electrodes used with Nafion®115 (b) and Aquivion®E87-05S (d).

The x-ray photoelectron spectroscopy was also performed to evaluate the surface chemical composition of the positive and negative electrodes after ageing tests and the results are shown in Fig. 7 and Table 2. Fig. 7a and b clearly show the presence of deposited Na_2SO_4 salts on the surface of both positive and negative aged electrodes. The negative aged electrodes (Fig. 7a) present C 1s and F 1s peaks derived from the activated carbon and PVDF binder, respectively, whereas Na 1s, S 2s and O 1s peaks come from the sodium sulphate of the electrolyte. In addition, some traces of titanium oxide (Ti $2p_{3/2}$) and silica (Si 2s) were also evidenced. The silica traces may come from some contamination present in the cell, while TiO_2 is likely due to a slight corrosion from the titanium cell plates. A similar consideration can be done for the positive aged electrodes (Fig. 7b), where the same chemical compounds together with the manganese oxides are observed. The F, Na, S elements were not further analysed at high resolution because they are not electrochemically active materials in the operating voltage of both SCs. On the other hand, although the oxygen is present in MnO_x, the O 1s spectra was also not further considered in this discussion because of the oxygen contribution occurs from multiple sources such as MnO_2, Na_2SO_4, H_2O, and the presence of oxygen-based functional groups on the carbon surfaces of CB, CNF, and the cotton textile used. Consequently, Mn $2p_{3/2}$ spectra were used to distinguish the main states of manganese oxidation (i. e. Mn^{4+}, Mn^{3+} and Mn^{2+}) and discern the presence of the three major components MnO_2, MnOOH/MnOONa and MnO in the fresh (Fig. 7c) and aged positive electrodes used with Nafion®115 (Fig. 7d) and Aquivion®E87-05S (Fig. 7e) membranes. Overall, multiple peaks are assigned to the different oxidation states of manganese oxide [27], though Mn^{3+} and Mn^{4+} species have to be added to the main peaks because they arise from the multiplet-splitting components of Mn 2p (IV) when an atom contains unpaired d electrons [44,45]. The main peak of manganese oxide appears at the binding energy of 642.8 ± 0.4 eV, which corresponds to MnO_2 (IV). Other two peaks with values of 641 ± 0.4 eV (Mn^{2+}) and 642 ± 0.4 eV for Mn^{3+} (MnOOH/MnOONa) were also found. Significantly, there were not observed any evident signs of degradation in the manganese oxide based electrodes from the comparison of the three high resolution Mn $2p_{3/2}$ spectra (Fig. 7c–e) and the survey analysis (Fig. 7b) for aged (Fig. 7d and e) and fresh samples (Fig. 7c), despite they were subjected to very stressful electrochemical tests for about 2–3 months. Moreover, the simultaneous co-existence of Mn^{4+}, Mn^{3+} and Mn^{2+} metal oxides, clearly confirms that these electrodes were not significantly altered after the prolonged tests. It must be reminded that the possible fast surface redox reactions produced in our MnO_2-based positive electrodes can be ascribed to reversible surface electrochemical reactions associated with adsorption/desorption of alkali metal cations such as Na^+ and protons H^+ [46], described by the following equation where C+ = Na^+, H^+, K^+:

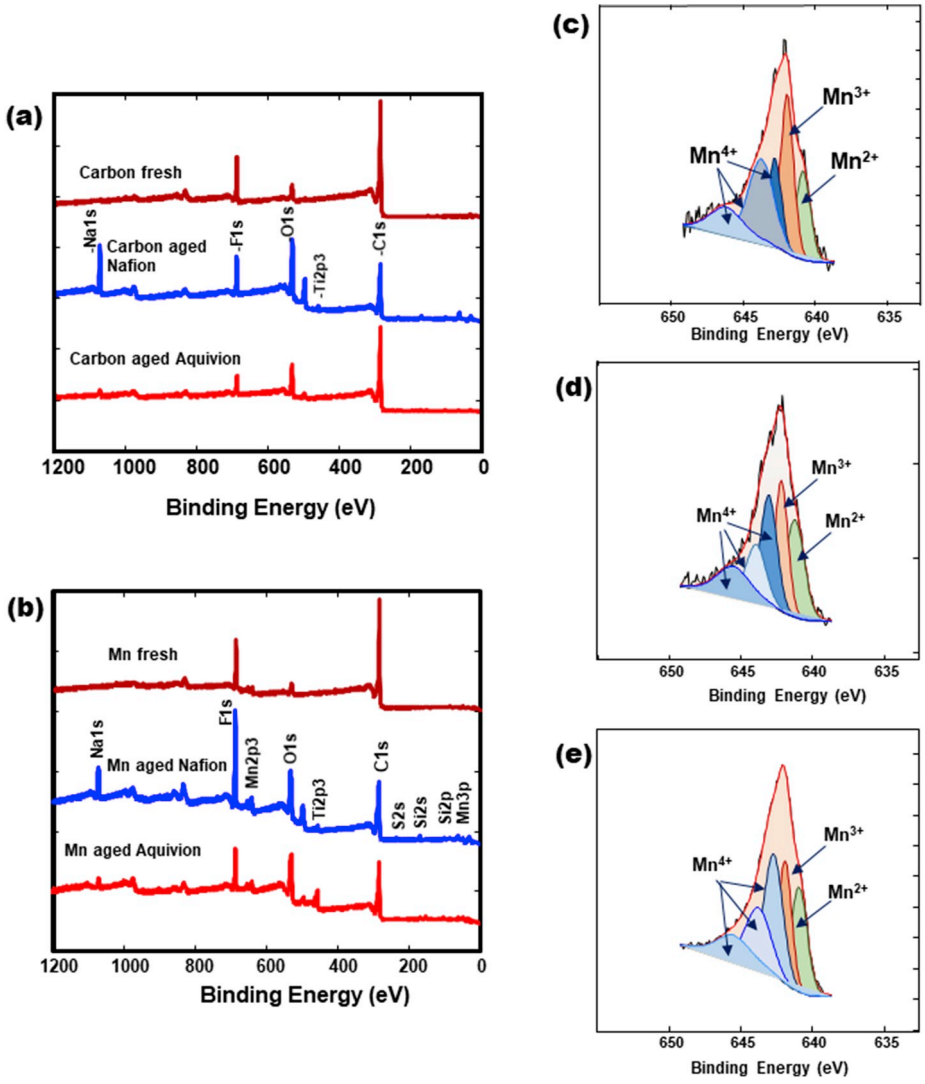

Fig. 7. XPS survey and deconvolution plots of fresh and aged electrodes. XPS of negative (a) and positive electrodes (b). Deconvolution of Mn $2p_{3/2}$ for MnO_x-fresh electrode (c), MnO_x aged Nafion®115 electrode (d), and MnO_x aged Aquivion®E87-05S electrode (e).

Table 2
XPS results of Mn $2p_{3/2}$ spectral fitting parameters: binding energy (eV) and percentage of total area for the fresh and aged electrodes.

Electrodes	Mn 2p3/2				
Peak	Peakl	Peak 2	Peak 3	Peak 4[a]	Peak 5[a]
BE (eV) compounds (valence)	641±0.4 MnO (II)	641±0.4 MnOOH MnOONa (III)	642.8±0.4 MnO_2 (IV)	643.8±0.4 MnO_2 (IV)	645.5±0.4 MnO_2 (IV)
Mn oxide fresh (%)	17.47	27.82	15.63	27.92	11.14
Mn oxide aged Cotton@Nafion (%)	22.84	21.10	29.24	17.87	8.95
Mn oxide aged Cotton@Aquivion (%)	25.49	23.49	24.18	14.41	12.33

[a] (Additional peaks are due to binding energy shifts and attributed to multiplet splitting structures).

$$MnO_2 + xC^+ + yH^+ + (x + y)e^- \leftrightarrow MnOOC_xH_y$$

This electrode mechanism, which involves a reversible redox reaction between IV and III Mn oxidation states, becomes more evident in the voltammograms of Fig. 4a and c with the appearance of humps with some deviation from rectangular shapes. This deviation is probably caused by the increased insertion of ions under the floating condition at the maximum voltage of 1.6 V, which could promote a higher electro-insertion of cations in the inner parts of the Mn electrodes.

In summary, the preserved morphology of the aged electrodes observed by the SEM images and the excellent electrochemical performance, demonstrate the lack of significant changes in both SCs. In this regard, a slight increase in their performance after 10 k and 15 k cycles and 140 h and 210 h of potentiostatic floating conditions at 1.6 V was observed, in contrast with the current state-of-art, which normally reports a performance decay after a few hundred (or thousands) of fast charge and discharge cycles [47–49].

The very significant results of our developed hybrid solid-state SC are also shown in the comparative plots of Fig. 8. The Cotton@Nafion SC worked perfectly for 10 k cycles and 140 h of potentiostatic floating at 1.6 V, after which the test was deliberately stopped, while the Cotton@Aquivion SC was subjected for 15 k cycles and 210 h of potentiostatic floating at 1.6 V before ending deliberately the test (Fig. 8a). The specific capacitances of both capacitors, obtained from the G-CD at 0.2 A g^{-1} for different number of cycles, started from values of about 105 F g^{-1} and then they increased until values of about 130 F g^{-1}. Thereafter, the capacitances remained constant and without any appreciable decay over that initial value until the end of the durability measurements, as it is evidenced by the solid lines in Fig. 8a. Furthermore, there was not observed any evident deterioration due to the corrosion phenomena in the current collector made of almost pure titanium (99.8%), normally observed in the positive current collector of SCs based on aqueous electrolytes [50,51]. In conclusion, our developed SCs work efficiently in neutral aqueous systems without any appreciable decay effects, despite the very harsh conditions to which electrodes, electrolytes and current collectors were subjected.

The Fig. 8b reports the voltage decay in the self-discharge behavior after 4 h of charging at constant voltage of 1.6 V of both aged SCs for 10 k cycles. This decrease of cell voltage can be caused by charge redistribution and various parasitic redox processes due to the presence of inorganic or organic impurities in the electrodes, which can produce undesired parallel chemical reactions, mass transport limitations and additional ohmic resistances [52–54]. In any case and despite the self-discharge rate is not completely eliminated in our SCs, it is small enough to be considered as negligible for practical devices.

The comparison of the electrochemical performance of SCs developed in this study with other supercapacitors based on textile-based electrodes reported in literature is summarized in Table 3. In our study, the highest specific capacitance of 132 F g^{-1} at 0.2 A g^{-1} was achieved with the Cotton@Nafion SC that showed an ionic resistance of 0.78 Ω cm^2, and an energy density of 11.55 Wh kg^{-1}. Our results are already remarkable when compared to similar asymmetric SCs reported in Table 3. Furthermore, they have shown low self-discharge rates and very good long-term durability under harsh cycling conditions, which are distinctive points of strength compared to the state-of-art for the design of future advanced solid-state SCs in neutral aqueous environments at operating voltages up to 1.6 V.

4. Conclusions

Two type of hybrid solid-state supercapacitors based on cotton fabric

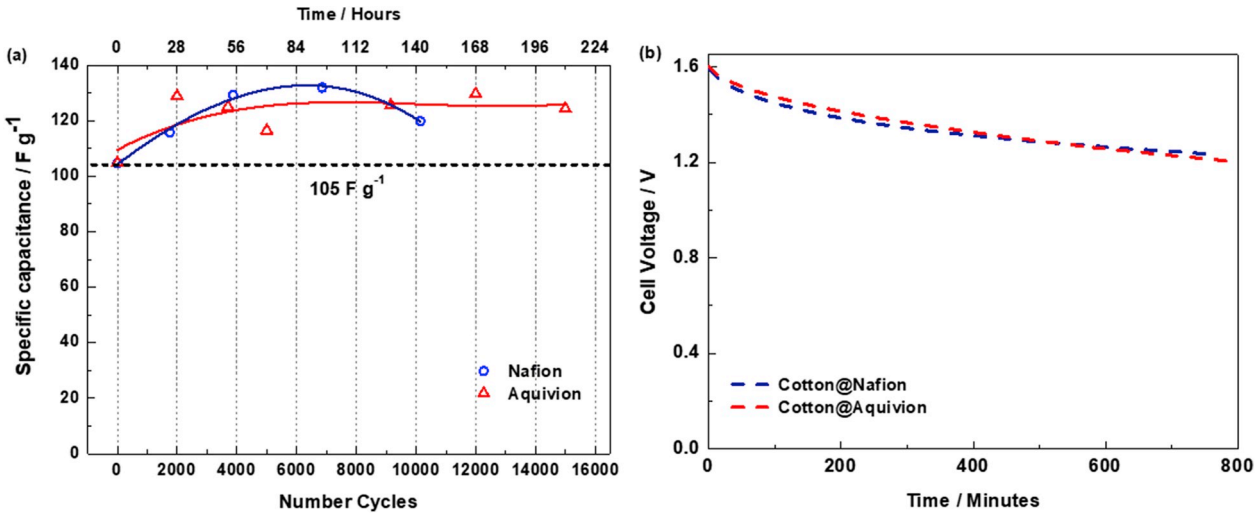

Fig. 8. Comparative results of SC with cycling life measurements. Specific capacitance as function of time and cycles (the solid lines are to guide the eyes) (a). Self-discharge rate after charging the SC for 4 h at 1.6 V (b).

Table 3
Performance comparative table of supercapacitors developed in this study with other Symmetric (S) and Asymmetric (A) flexible SC.

SC type	Substrate	Active materials	Electrolyte	Separator	Working voltage (V)	Capacitance (F g^{-1}) at current	Energy density (Wh kg^{-1})	Retention	Refs
S	Cotton Fabric	SWCNT, MnO_2	2 M Li_2SO_4	Cotton Fabric	0.8	170 1 mA/cm^2	–	100% 35 K Cycles	[17]
S	Cotton Fabric	GO	2 M $EMIMBF_4$/ acetonitrile	Cotton Fabric	2	18.3 0.1 A/g	12.3	93% 1.5 K Cycles	[6]
A	Carbon Fabric	MnO_2, Fe_2O_3	PVA/LiCl	–	1.6	91.3 2 mA/cm^2	32.5	"Good" 5 K Cycles	[23]
S	Cotton Fabric	Ni, MWCNT, rGO	5 M LiCl	Cotton Fabric	0.8	262 0.84 A/g	–	118% 10 K Cycles	[19]
S	Cotton Fabric	Activated Carbon (AC)	1 M Li_2SO_4	PTFE membrane	1	90 0.25 A/g	–	92% 10K Cycles	[55]
S	Cotton Fabric	PPy	2 M NaCl	–	0.8	325 1 A/g	24.7	63% 500 Cycles	[18]
A	Activated Cotton Textile (ACT)	ACT, MnO_2	1 M Na_2SO_4	Whatman Paper	2	120 1 mA/cm^2	16.7[a]	97.5% 1K Cycles	[13]
A	ACT	$NiCo_2O_4$, $NiCo_2O$	PVA/KOH	–	1.6	60 100 mA/cm^2	21.3[a]	100% 1K Cycles	[14]
A	Carbon Cloth (CC)	MnO_2, CC	PVA/LiCl	–	2.0	178 4 mA/cm^2	25	96% 20 K Cycles	[56]
A	Carbon Nanofiber Paper	MnO_2, Bi_2O_3	1 M Na_2SO_4	Filter Paper	1.8	100.8 1.5 mA/cm^2	11.3	85% 4 K Cycles	[20]
S	Carbon Cloth	MultiScale Porous Carbon	0.5 M H_2SO_4, 1 M KOH	Porous Paper	1.4	177 mF/cm^2 1 mA/cm^2	0.72 mWh/ cm^3	85% 30 K Cycles	[3]
S	Flexible Stainless-Steel	AC	1 M Li_2SO_4	Li_2SO_4 Gel Electrolyte	2.1	–	26.5	94% 10 K Cycles	[57]
A	Nickel Foam, Carbon Cloth	NiO, NiOOH, PPy	4 M KOH	Filter Paper	1.4	0.613 mAh/cm^2	4.12 mWh/ cm^3	88% 5 K Cycles	[58]
A	Carbon Cloth	rGO, MnO_2	PVA/Na_2SO_4	–	2	120 mF/cm^2	64 μWh/cm^3	95% 10 K Cycles	[5]
S	Graphite Paper	MnO_2	1 M Na_2SO_4	Porous Paper	1	76.1 mF/cm^3 0.5 mA/cm^2	10.6 mWh/ cm^3	93.6% 1 K Cycles	[59]
S	–	3D rGO	PVA/H_3PO_4	–	1	81 0.5 A/g	11.5	94.5% 1 K Cycles	[60]
S	Polyester Textile	rGO, PANI	PVA/H_3PO_4	–	0.8	152 0.5 mA/cm^2	–	85.9% 1 K Cycles	[19]
A	Cotton textile	CNF + AC + MnO_2	Nafion-Na^+/1 M Na_2SO_4	Nafion	1.6	132 @ 0.5 A/g	11.7	126% 10 K cycles + (140 h @ 1.6 V)	**This work**
A	Cotton textile	CNF + AC + MnO_2	Aquivion- Na^+/ 1 M Na_2SO_4	[a]Aquivion	1.6	130 @ 0.2 A/g	11.55	125% 15 K cycles + (210 h- 1.6 V)	**This work**

[a] Energy density is derived from capacitance of a single electrode

electrodes were designed and analysed in this work. One SC was assembled with *Nafion® 115* and the other SC with *Aquivion® E87-05S* polymer electrolyte. Furthermore, a new lifetime assessment methodology, consisting of the combination of galvanostatic charge/discharge and potentiostatic floating tests, was designed and carried out for the first time in order to get insight on the durability of both SCs under harsh test environments. The voltammograms and charge–discharge profiles (at initial conditions) of the two different SC showed the typical rectangular-shape voltammetries and symmetric triangular shapes G-CD curves of quasi-ideal electric double layer capacitors with very interesting capacitive performances (≈105 F g^{-1}) in neutral aqueous environment at cell voltage of 1.6 V, which are comparable to similar results found in literature but with the difference that our SCs were produced with very simple and scalable methods and a majority of low-cost materials such as cotton fabric, activated carbon, carbon black and MnO_2 nanoparticles. The designed SCs showed very low self-discharge rates and even an increase in their capacitances of 25% (from 105 to 132 F g^{-1}) during long-term durability tests. In particular, the SC based on *Nafion® 115* membrane was subjected to the potentiostatic floating condition of 1.6 V for more than 10 K cycles and 140 h, whereas the SC based on *Aquivion® E87-05S* membrane achieved 15 k cycles and 210 h at 1.6 V in perfect operation. The post-mortem analysis (e.g. SEM and XPS) made on the fresh and aged electrodes did not show significant structural changes in their morphologies, which means that the MnO_2 nanoparticles and activated carbon utilized were not degraded, despite they have been subjected to very stringent testing conditions.

Conflicts of interest

The authors declare no conflict of interest.

Acknowledgments

This work was supported by Project UID/CTM/00264/2019 of 2C2T – Centro de Ciência e Tecnologia Têxtil, funded by National Founds through FCT/MCTES. This research was also partially supported by the Cost Action 15107, Grant No. ECOST-STSM-CA15107-300118-092731. The authors acknowledge Mr. A. Brigandì (CNR-ITAE) and Mr. G. Monforte for their help with electrochemical tests and XPS analysis, respectively and Mr. André Paiva (2C2T) for the graphic design of Fig. 3.

References

[1] U. Gulzar, S. Goriparti, E. Miele, T. Li, G. Maidecchi, A. Toma, F. De Angelis, C. Capiglia, R.P. Zaccaria, J. Mater. Chem. 4 (2016) 16771–16800.
[2] P. Simon, Y. Gogotsi, Nat. Mater. 7 (2008) 845–854.
[3] M. Yu, D. Lin, H. Feng, Y. Zeng, Y. Tong, X. Lu, Angew. Chem. Int. Ed. 56 (2017) 5454–5459.

[4] S. Kumar, M. Nehra, D. Kedia, N. Dilbaghi, K. Tankeshwar, K.H. Kim, Prog. Energy Combust. Sci. 64 (2018) 219–253.
[5] H. Jeon, J.M. Jeong, S.B. Hong, M. Yang, J. Park, D.H. Kim, S.Y. Hwang, B.G. Choi, Electrochim. Acta 280 (2018) 9–16.
[6] W.W. Liu, X.B. Yan, J.W. Lang, C. Peng, Q.J. Xue, J. Mater. Chem. 22 (2012) 17245–17253.
[7] X. Guo, S. Zheng, G. Zhang, X. Xiao, X. Li, Y. Xu, H. Xue, H. Pang, Energy Storage Mater. 9 (2017) 150–169.
[8] X. Chen, R. Paul, L. Dai, Natl. Sci. Rev. 4 (2017) 453–489.
[9] Q. Meng, K. Cai, Y. Chen, L. Chen, Nano Energy 36 (2017) 268–285.
[10] B.E. Conway, W.G. Pell, J. Solid State Electrochem. 7 (2003) 637–644.
[11] M. Meller, J. Menzel, K. Fic, D. Gastol, E. Frackowiak, Solid State Ionics 265 (2014) 61–67.
[12] T.H. Wu, D. Hesp, V. Dhanak, C. Collins, F. Braga, L.J. Hardwick, C.C. Hu, J. Mater. Chem. 3 (2015) 12786–12795.
[13] L. Bao, X. Li, Adv. Mater. 24 (2012) 3246–3252.
[14] Z. Gao, N. Song, Y. Zhang, X. Li, RSC Adv. 5 (2015) 15438–15447.
[15] S. Seyedin, M.S. Romano, A.I. Minett, J.M. Razal, Sci. Rep. 5 (2015) 14946.
[16] K. Jost, D. Stenger, C.R. Perez, J.K. McDonough, K. Lian, Y. Gogotsi, G. Dion, Energy Environ. Sci. 6 (2013) 2698–2705.
[17] L. Hu, M. Pasta, F. La Mantia, L. Cui, S. Jeong, H.D. Deshazer, J.W. Choi, S.M. Han, Y. Cui, Nano Lett. 10 (2010) 708–714.
[18] J. Xu, D. Wang, L. Fan, Y. Yuan, W. Wei, R. Liu, S. Gu, W. Xu, Org. Electron.: Phys. Mater. Appl. 26 (2015) 292–299.
[19] Y. Yang, Q. Huang, L. Niu, D. Wang, C. Yan, Y. She, Z. Zheng, Adv. Mater. 29 (2017) 1606679.
[20] H. Xu, X. Hu, H. Yang, Y. Sun, C. Hu, Y. Huang, Adv. Energy Mater. 5 (2015) 7484–7539.
[21] Q. Chen, X. Li, X. Zang, Y. Cao, Y. He, P. Li, K. Wang, J. Wei, D. Wu, H. Zhu, RSC Adv. 4 (2014) 36253–36256.
[22] X. Lu, M. Yu, G. Wang, Y. Tong, Y. Li, Energy Environ. Sci. 7 (2014) 2160–2181.
[23] P. Yang, Y. Ding, Z. Lin, Z. Chen, Y. Li, P. Qiang, M. Ebrahimi, W. Mai, C.P. Wong, Z.L. Wang, Nano Lett. 14 (2014) 731–736.
[24] H. Sun, S. Xie, Y. Li, Y. Jiang, X. Sun, B. Wang, H. Peng, Adv. Mater. (2016) 8431–8438.
[25] F. Lufrano, P. Staiti, Electrochim. Acta 49 (2004) 2683–2689.
[26] F.A. Zakil, S.K. Kamarudin, S. Basri, Renew. Sustain. Energy Rev. 65 (2016) 841–852.
[27] A.J. Paleo, P. Staiti, A. Brigandì, F.N. Ferreira, A.M. Rocha, F. Lufrano, Energy Storage Mater. 12 (2018) 204–215.
[28] P. Staiti, F. Lufrano, Electrochim. Acta 55 (2010) 7436–7442.
[29] L. Zhang, Q. Chen, X. Han, Q. Zhang, J. Clust. Sci. 29 (2018) 1089–1098.
[30] E.S. Ilton, J.E. Post, P.J. Heaney, F.T. Ling, S.N. Kerisit, Appl. Surf. Sci. 366 (2016) 475–485.
[31] I. Roger, M.A. Shipman, M.D. Symes, Nat. Rev. Chem. 1 (2017), 0003.
[32] J. Liu, D. Zhu, T. Ling, A. Vasileff, S.Z. Qiao, Nano Energy 40 (2017) 264–273.
[33] T. Brousse, D. Bélanger, J.W. Long, J. Electrochem. Soc. 162 (2015) A5185–A5189.
[34] Y. Shao, M.F. El-Kady, J. Sun, Y. Li, Q. Zhang, M. Zhu, H. Wang, B. Dunn, R. B. Kaner, Chem. Rev. 118 (2018) 9233–9280.
[35] N. Jabeen, Q. Xia, S.V. Savilov, S.M. Aldoshin, Y. Yu, H. Xia, ACS Appl. Mater. Interfaces 8 (2016) 33732–33740.
[36] G. Yu, L. Hu, N. Liu, H. Wang, M. Vosgueritchian, Y. Yang, Y. Cui, Z. Bao, Nano Lett. 11 (2011) 4438–4442.
[37] F. Lufrano, P. Staiti, Energy Fuels 24 (2010) 3313–3320.
[38] B.E. Conway, Electrochemical behavior at porous electrodes; applications to capacitors, in: B.E. Conway (Ed.), Electrochemical Supercapacitors, Springer, Boston, MA (USA), 1999, pp. 377–416.
[39] P.W. Ruch, D. Cericola, A. Foelske-Schmitz, R. Kötz, A. Wokaun, Electrochim. Acta 55 (2010) 4412–4420.
[40] D. Weingarth, H. Noh, A. Foelske-Schmitz, A. Wokaun, R. Kötz, Electrochim. Acta 103 (2013) 119–124.
[41] P. Ratajczak, K. Jurewicz, F. Béguin, J. Appl. Electrochem. 44 (2014) 475–480.
[42] T.H. Wu, Y.H. Chu, C.C. Hu, L.J. Hardwick, Electrochem. Commun. 27 (2013) 81–84.
[43] M. Rajkumar, C.T. Hsu, T.H. Wu, M.G. Chen, C.C. Hu, Prog. Nat. Sci.: Mater. Int. 25 (2015) 527–544.
[44] M.C. Biesinger, B.P. Payne, A.P. Grosvenor, L.W.M. Lau, A.R. Gerson, R.S.C. Smart, Appl. Surf. Sci. 257 (2011) 2717–2730.
[45] H.W. Nesbitt, D. Banerjee, Am. Mineral. 83 (1998) 305–315.
[46] M. Toupin, T. Brousse, D. Bélanger, Chem. Mater. 16 (2004) 3184–3190.
[47] T. Brousse, et al., Materials for electrochemical capacitors, in: C. Breitkopf, K. Swider-Lyons (Eds.), Handbook of Electrochemical Energy, Springer, Berlin, Heidelberg, 2017, pp. 495–561.
[48] W. Wei, X. Cui, W. Chen, D.G. Ivey, J. Power Sources 186 (2009) 543–550.
[49] T. Zhai, S. Xie, M. Yu, P. Fang, C. Liang, X. Lu, Y. Tong, Nano Energy 8 (2014) 255–263.
[50] P. Ratajczak, K. Jurewicz, P. Skowron, Q. Abbas, F. Béguin, Electrochim. Acta 130 (2014) 344–350.
[51] B. Evanko, S.J. Yoo, J. Lipton, S.E. Chun, M. Moskovits, X. Ji, S.W. Boettcher, G. D. Stucky, Energy Environ. Sci. 11 (2018) 2865–2875.
[52] L. García-Cruz, P. Ratajczak, J. Iniesta, V. Montiel, F. Béguin, Electrochim. Acta 202 (2016) 66–72.
[53] X. Wang, R.S. Chandrabose, S.E. Chun, T. Zhang, B. Evanko, Z. Jian, S. W. Boettcher, G.D. Stucky, X. Ji, ACS Appl. Mater. Interfaces 7 (2015) 19978–19985.
[54] H.A. Andreas, J.M. Black, A.A. Oickle, Electrochim. Acta 140 (2014) 116–124.
[55] K. Jost, C.R. Perez, J.K. McDonough, V. Presser, M. Heon, G. Dion, Y. Gogotsi, Energy Environ. Sci. 4 (2011) 5060–5067.
[56] H. Wang, C. Xu, Y. Chen, Y. Wang, Energy Storage Mater. 8 (2017) 127–133.
[57] J. Wei, J. Zhou, S. Su, J. Jiang, J. Feng, Q. Wang, ChemSusChem 11 (2018) 3410–3415.
[58] H. Khani, T.J. Dowell, D.O. Wipf, ACS Appl. Mater. Interfaces 10 (2018) 21262–21280.
[59] W. Qi, R. Lv, B. Na, H. Liu, Y. He, N. Yu, ACS Sustain. Chem. Eng. 6 (2018) 4739–4745.
[60] T. Purkait, G. Singh, D. Kumar, M. Singh, R.S. Dey, Sci. Rep. 8 (2018) 640.